Research Article

Journal of RAMAN SPECTROSCOPY

Received: 22 April 2009 Accepted: 1 June 2009 Published online in Wiley Interscience: 31 July 2009

(www.interscience.wiley.com) DOI 10.1002/jrs.2371

Gas-phase structure and new vibrational study of methyl trifluoroacetate ($CF_3C(O)OCH_3$)

María E. Defonsi Lestard,[a] María E. Tuttolomondo,[a] Eduardo L. Varetti,[b†] Derek A. Wann,[c] Heather E. Robertson,[c] David W. H. Rankin[c] and Aida Ben Altabef[a*†]

The molecular structure of methyl trifluoroacetate ($CF_3C(O)OCH_3$) has been determined in the gas phase from electron-diffraction data supplemented by *ab initio* (MP2) and DFT calculations using different basis sets. Experimental data revealed an *anti* conformation with a dihedral angle θ (CCOC) = 180°. Quantum mechanical calculations indicate the possible existence of two conformers, differing by a rotation about the C(O)–O bond. The global minimum represents a C_s-symmetric structure in which the CF_3 group has the *anti* orientation with respect to the CH_3 group, but there is another potential minimum, much higher in energy, representing a C_s-symmetric structure with a *cis* conformation. The preference for the *anti* conformation was studied using the total energy scheme and the natural bond orbital (NBO) partition scheme. Additionally, the total potential energy has been deconvoluted using a six-fold decomposition in terms of a Fourier-type expansion, showing that the electrostatic and steric contributions are dominant in stabilizing the *anti* conformer. Infrared spectra of $CF_3C(O)OCH_3$ were obtained for the gaseous and liquid phases, while the Raman spectrum was recorded for the liquid phase. Harmonic vibrational frequencies and a scaled force field have been calculated, leading to a final root mean-square deviation of 9 cm^{-1} when comparing experimental and calculated frequencies.

Supporting information may be found in the online version of this article.

Keywords: methyl trifluoroacetate; gas electron diffraction; *ab initio* calculations; DFT calculations; infrared spectra; Raman spectra

Introduction

The trifluoromethyl group is a highly important substituent in the field of organic chemistry. Over the past two decades, the number of new organofluorine compounds has increased tremendously because of their different, sometimes improved, properties compared with nonfluorinated analogues.[1] The powerful electron-withdrawing ability and the relatively small size of the trifluoromethyl group can bring remarkable changes in the physical, chemical and biological properties of molecules, making them suitable for diverse applications in the areas of materials science and the pharmaceutical and agrochemical industries.[2,3] It is therefore desirable to investigate and understand the fundamental properties of such fluorinated organic compounds. In that way, the studies made on trifluoroethyl trifluoroacetate[4] in this laboratory have been extended to include methyl trifluoroacetate, in order to gain structural information relating to possible conformational isomerism and vibrational information relating to the force constants.

Although a microwave study of $CF_3C(O)OCH_3$ was made previously by Jones *et al*.,[5] who concluded that the gas-phase structure adopted a planar *anti* conformation, no further structural parameters were determined. However, the determination of accurate bond lengths, bond angles and torsion angles are essential for comparison with similar, but more complex, structures. The full structure of $CF_3C(O)OCH_3$ has now been determined by gas electron diffraction (GED).

Methyl trifluoroacetate has been subjected previously to vibrational analyses by means of infrared and Raman spectroscopies.[5–7] In the present work, new spectra were obtained and previous assignment of bands to the normal modes of vibration were revised to serve as a basis for the calculation of a scaled quantum mechanical (SQM) force field, using the methodology of Pulay *et al*.[8]

In addition, the energy of the system in relation to the internal rotation about the C(O)–O bond has been calculated using various computational approaches (both *ab initio* and DFT) and fitted to a six-fold Fourier-type expansion. This methodology has allowed an analysis of the nature of the potential function which explains the preferred conformation of the molecule. The study has been completed with a natural bond orbital (NBO) analysis, to assess the significance of hyperconjugative interactions on such conformation.

* *Correspondence to: Aida Ben Altabef, INQUINOA, CONICET, Instituto de Química Física, Facultad de Bioquímica, Química y Farmacia, Universidad Nacional de Tucumán, San Lorenzo 456, T4000CAN Tucumán, R. Argentina. E-mail: altabef@fbqf.unt.edu.ar*

† *Members of the Carrera del Investigador Científico, CONICET, R. Argentina.*

a *INQUINOA, CONICET, Instituto de Química Física, Facultad de Bioquímica, Química y Farmacia, Universidad Nacional de Tucumán, San Lorenzo 456, T4000CAN Tucumán, R. Argentina*

b *Centro de Química Inorgánica (CEQUINOR, CONICET-UNLP), Departamento de Química, Facultad de Ciencias Exactas, Universidad Nacional de La Plata, C. Correo 962, 1900 La Plata, R. Argentina*

c *School of Chemistry, University of Edinburgh, Edinburgh, EH9 3JJ, UK*

Experimental

A sample of methyl trifluoroacetate (Sigma-Aldrich) was used without further purification for both diffraction and spectroscopy experiments. All handling was performed under dry nitrogen to protect the sample from atmospheric humidity.

Gas-phase electron diffraction

Data were collected for $CF_3C(O)OCH_3$ on Kodak Electron Image films using the Edinburgh GED apparatus.[9] The accelerating voltage was held at approximately 40 keV, yielding electrons with a wavelength of approximately 6 pm. Data were collected at two nozzle-to-film distances to increase the range of angles over which scattering was observed. The nozzle was at room temperature (approximately 293 K), while the sample was cooled to 243 K for both the long and short nozzle-to-film distances.

The scattering patterns were converted into digital form using an Epson Expression 1680 Pro flatbed scanner and an extraction program described elsewhere.[10] Data reduction and least-squares refinements were performed using the ed@ed v2.4 program,[11] employing the scattering factors of Ross *et al.*[12] The weighting points for the off-diagonal weight matrices, correlation parameters and scale factors for both nozzle-to-film distances are given in Table S1 (Supporting Information).

Infrared and Raman spectroscopy

Infrared spectra of $CF_3C(O)OCH_3$ in the gaseous and liquid phases were recorded in the 4000–400 cm^{-1} range at room temperature using a Perkin-Elmer GX1 FTIR instrument. A glass cell with a 10-cm optical path and KBr windows was used to obtain the gas-phase spectrum, whereas for the liquid spectrum the substance was held as a thin film between KBr windows. The FIR spectra in the region below 500 cm^{-1} of the gas substance were recorded on a Nexus Nicolet instrument equipped with a deuterated triglycine sulfate (DTGS) detector, using a 10-cm glass cell provided with silicon windows.

The polarized Raman spectrum of the liquid at room temperature was obtained with an FT-Raman RFS 100/S spectrometer using the 1064 nm line from a Nd : YAG laser for excitation.

Computational details

Some calculations were performed using the resources of the U.K. National Service for Computational Chemistry Software (NSCCS),[13] while others were carried out on a PC, both running the Gaussian 03 suite of programs.[14]

Potential energy curves were calculated at the MP2 and B3LYP levels with the 6-311++G(d,p) basis set, and two minima were identified by rotating about the C(O)–O bond; the global minimum represents a C_s-symmetric (*anti*) structure and another, higher in energy, represents a C_s-symmetric (*cis*) structure (Fig. 1). Geometry optimizations were first performed for both conformers at the MP2[15] and DFT methods with the 6-311G(d)[16] and 6-311++G(d,p)[17] basis sets. DFT methods used Becke's B3 hybrid exchange functional[18] and the Lee-Yang-Parr non-local correlation functional (LYP).[19,20] All calculations were spin-restricted and frozen-core.

Vibrational wavenumbers were calculated from analytic second derivatives to check that the optimized structures represented minima on the potential energy surface. Harmonic force constants calculated at the B3LYP/6-311++G(d,p) level were subsequently

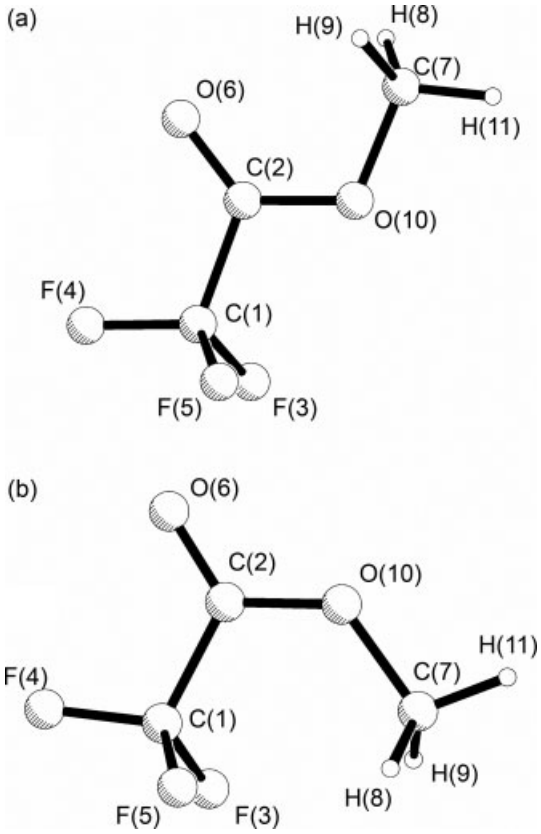

Figure 1. Molecular structure, including numbering scheme, of (a) the *anti* (C_s symmetry) conformer and (b) the *cis* (C_s symmetry) conformer of $CF_3C(O)OCH_3$.

used, along with the program SHRINK,[21] to obtain initial amplitudes of vibration and also to calculate curvilinear distance correction terms for use in the GED refinement. The structure obtained from the refinement is therefore of the type r_{h1}.

The potential energies associated with the CCOC dihedral angle were calculated at the B3LYP and MP2 levels using the 6-311++G(d,p) basis set. In such calculations, the torsion angle was frozen whereas all other parameters were allowed to relax. The total energy curve was constructed in steps of 5° or 10° using default convergence criteria as implemented in the Gaussian programs.

Natural bond orbital (NBO) calculations were performed at the B3LYP/6-311++G(d,p) level using the NBO 3.0 code[22] as implemented in the Gaussian 03 package.

The harmonic force field in Cartesian coordinates calculated at the B3LYP/6-311++G(d,p) level was transformed to a set of natural internal (local symmetry) coordinates[23] via the B matrix,[24] which was obtained using a standard program. Subsequently, a SQM force field was obtained using the scheme of Pulay *et al.*[8] in which the diagonal force constants are multiplied by scale factors $f_i, f_j, \ldots$ and the corresponding interaction constants are multiplied by $(f_i.f_j)^{1/2}$, and adjusting the scale factors to reproduce the experimental frequencies as well as possible. No empirical correction of the theoretical geometry was used. The potential energy distribution was then calculated with the resulting SQM force field. The force field for the *anti* conformer, scaling and determination of the potential energy distribution were performed with the program FCARTP.[25] The atomic displacements given by the Gaussian 03 program for each vibrational mode were used to

Journal of RAMAN SPECTROSCOPY

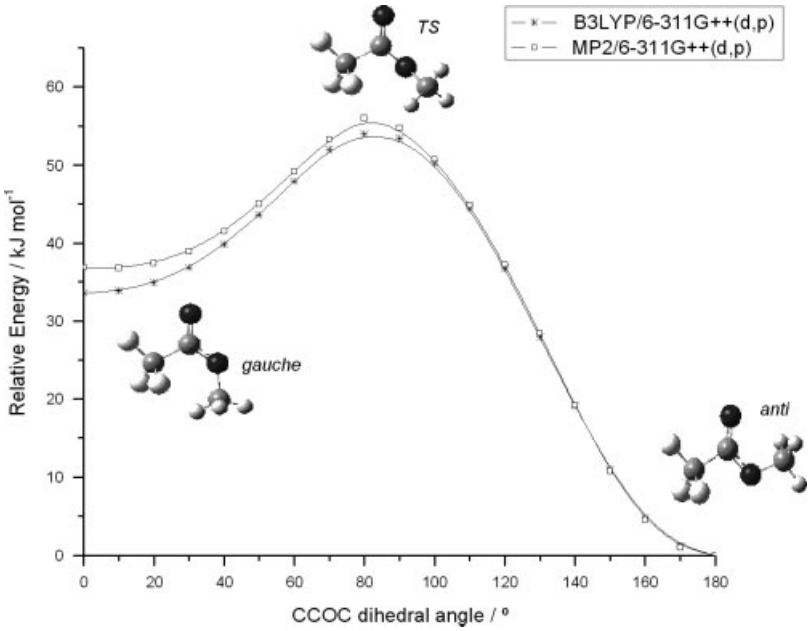

Figure 2. Torsional potential about the C(O)–O bond of $CF_3C(O)OCH_3$, calculated at different levels of theory.

understand the nature of the molecular vibrations qualitatively; for that purpose, the corresponding data were represented graphically using the GaussView program.[26]

Results and Discussion

Quantum chemical calculations

Two stable conformations, both with C_s symmetry (Fig. 1), were identified with every combination of level of theory and basis set that was used. Calculated geometrical parameters for $CF_3C(O)OCH_3$ are listed in Table S2 (Supporting Information).

The potential energy scans about the (O)C–O bond at the B3LYP and MP2 levels using the 6-311++G(d,p) basis set are shown in Fig. 2. There is good agreement between the MP2 and B3LYP methods, identifying two different minima, both with C_s symmetry. When the dihedral angle was 0° (*cis*), the energy was considerably higher than when the angle was 180° (*anti*). Table 1 lists the total energies for both conformers from calculations made at different levels of theory. Energy data show that the MP2 calculation increases the energy difference between the conformers, as does augmentation of the basis sets with diffuse and polarization functions.

Internal barrier decomposition schemes

The study of the nature of the rotation barrier about the (O)C–O bond in terms of hyperconjugative, steric and electrostatic interactions leads us to the foundations of the stabilization of the different conformers. The total energy curve for the target torsion angle was calculated in 10° steps in the range 0 to 180°, allowing all geometrical parameters to relax except for the one being scanned. The potential energy function $V(\theta)$, describing the internal rotation of one part of the molecule (rotor) relative to the remainder (framework), may be expanded as a sixth-order Fourier series:

$$V(\theta) = \sum_{i=1}^{6} \frac{1}{2} V_{iN} (1 - \cos\ iN\theta) \quad (1)$$

where θ is the angle of rotation and N, the symmetry number, is equal to 1. No contributions to torsional energies from zero-point energy were taken into account.

The decomposition of the total energy function and the analysis of the different terms V_i have previously been shown to be a simple way of analyzing the stabilization of different conformations in molecular systems.[27–31] Table S3 (Supporting Information) lists the V_i coefficients calculated for $CF_3C(O)OCH_3$ using the MP2 and B3LYP methods with the 6-311++G(d,p) basis set; these values show a good correlation between both methods. With their large values, V_1 and V_2 are the main contributions to the rotational barrier, with $V_2 > V_1 > V_3, V_4$. For both molecules, V_5 and V_6 are less significant when deconvoluting the potential energy curve. V_1 usually accounts for interactions between local dipoles and steric interactions and has a large value showing that there is a strong preference of the molecule for a 180° geometry over a 0° one. V_2 is usually associated with conjugative and hyperconjugative effects that have a periodicity of 180°. V_2 is large and positive, indicating that the contribution of the hyperconjugative effect

Table 1. Calculated energies for both conformers of $CF_3C(O)OCH_3$ at different levels of theory

Method	Basis set	*E*/Hartrees		ΔE/kJ mol^{-1}
		anti	*cis*	
B3LYP	6-31G(d)	−566.09098	−566.08143	25.1
B3LYP	6-311G(d,p)	−566.26065	−566.25047	26.7
B3LYP	6-311++G(d,p)	−566.27836	−566.26556	33.6
MP2	6-311++G(d,p)	−564.98720	−564.97319	36.7
MP2	6-31G(d,p)	−564.96089	−564.94736	35.5
MP2	6-31G(d)	−564.64151	−564.62840	34.4

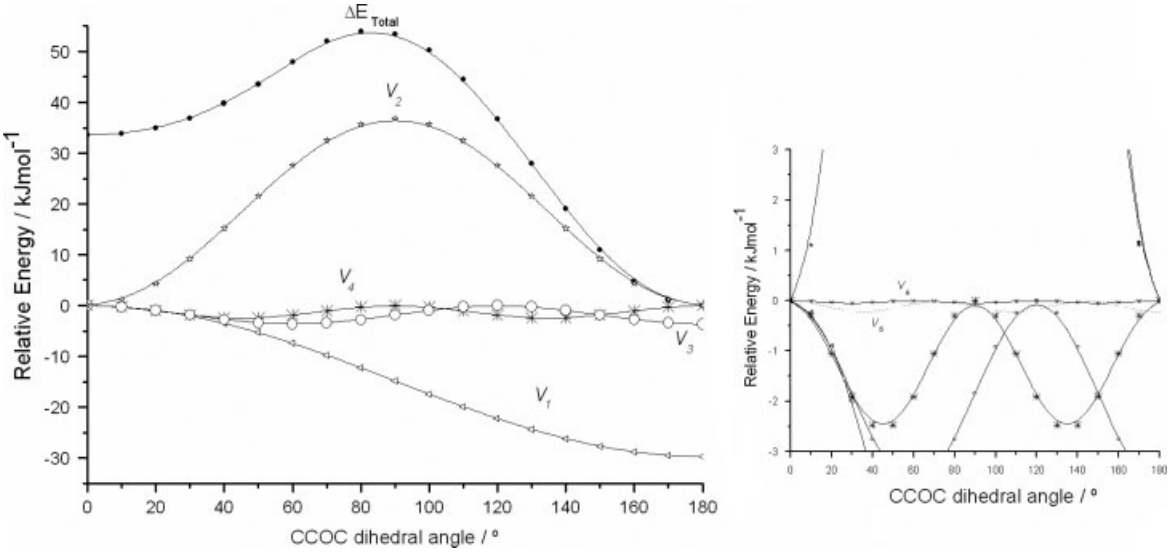

Figure 3. Fourier decomposition of the potential function $V(\theta)$ for $CF_3C(O)OCH_3$ calculated using the B3LYP method with the 6-311++G(d,p) basis set. On the right is an enlargement of the region containing V_5 and V_6.

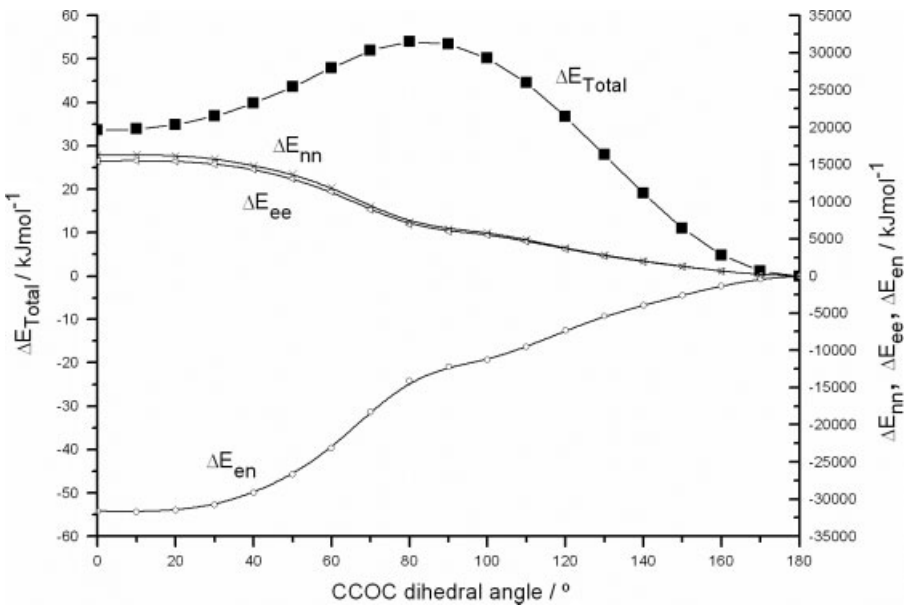

Figure 4. Dependence of attractive (ΔE_{ne}) and repulsive (ΔE_{nn} and ΔE_{ee}) energy increments on the CCOC dihedral angle in $CF_3C(O)OCH_3$, calculated at the B3LYP/6-311++G(d,p) level.

stabilizes the *anti* ($\theta = 180^\circ$) and *cis* ($\theta = 0^\circ$) conformers of $CF_3C(O)OCH_3$.

The remaining terms involve steric and electrostatic interactions.[27–31] Fig. 3 shows the Fourier decomposition of the total energy function calculated at the B3LYP level of theory with the 6-311++G(d,p) basis set. In order to confirm the contributions of the different terms in the Fourier decomposition, we have performed an investigation of the energy barrier based on the partition offered by the equation:

$$\Delta E = \Delta E_{nn} + \Delta E_{en} + \Delta E_{ee} + \Delta E_k \quad (2)$$

where ΔE is the total energy change between structures of different geometries, ΔE_{nn} is the energy change for nuclear repulsion, ΔE_{en} for electron–nuclear attraction, ΔE_{ee} for electron repulsion and ΔE_k is the kinetic energy. It can be seen that this equation describes the total energy change as the sum of all potential and kinetic contributions.

Table S4 (Supporting Information) illustrates the fact that the repulsive terms, E_{ee} and E_{nn}, are larger in the less stable conformation than they are for the more stable *anti* conformer. More detailed results for the energy as a function of the CCOC torsion are shown in Fig. 4. It can be seen that the repulsive terms E_{ee} and E_{nn} as functions of the torsion angle show the same trend as V_1, which indicates that V_1 accounts for the repulsive non-bonding interactions that favor the *anti* conformer stabilization.

For a rigorous analysis of the role of conjugative and hyperconjugative interactions in the stabilization of the different conformers, an NBO analysis was carried out. Following this scheme, the energy barrier $\Delta E_{barrier}$ can be written as a function of

Table 2. Important hyperconjugative interactions/kJ mol^{-1} for $CF_3C(O)OCH_3$ calculated at the B3LYP/6-311++G(d,p) level

	cis ϕ[C(1)O(10)C(2)C(7)] $= -0.5^\circ$	*anti* ϕ[C(1)O(10)C(2)C(7)] $= 180.0^\circ$
LP O(6) [a] $\rightarrow \sigma^*$ C(1)–C(2)	116.9	113.7
LP O(6) $\rightarrow \sigma^*$ C(2)–O(10)	130.8	134.3
LP O(6) $\rightarrow \sigma^*$ C(7)–H(11)	–	2.3
LP O(10) $\rightarrow \sigma^*$ C(2)–O(6)	209.1	250.3
LP O(10) $\rightarrow \sigma^*$ C(7)–H(8)	18.4	19.8
LP O(10) $\rightarrow \sigma^*$ C(7)–H(9)	17.4	19.8
LP O(10) $\rightarrow \sigma^*$ C(7)–H(11)	9.2	9.2
LP O(10) $\rightarrow \sigma^*$ C(1)–C(2)	27.8	7.5
Total	529.6	556.9

[a] LP denotes lone pair of electrons in the oxygen atom, designed with the number of Fig. 1.

bond strength, hyperconjugation and steric repulsion:

$$\Delta E_{barrier} = \Delta E_{Lewis} + \Delta E_{deloc} = \Delta E_{struct} + \Delta E_{exc} + \Delta E_{deloc} \quad [3]$$

where ΔE_{struct} takes into account Coulomb and bond energy changes in the classical structure, ΔE_{exc} (known as the Pauli exchange (or steric) repulsion energy) accounts for the non-Coulomb energy changes arising from the Pauli exclusion principle and ΔE_{deloc} describes the hyperconjugative stabilization.

Table S5 (Supporting Information) presents the contributions due to the localized electron density (E_{Lewis}) and to the delocalized electron density (E_{deloc}) to the rotation barrier around the C(O)–O bond at the B3LYP/6-311++G(d,p) level. This table shows how the Lewis energy is smaller for the *anti* conformer than the *cis* conformer. The Lewis energy difference ΔE_{Lewis} is a measure of molecular stability in the absence of the hyperconjugation interaction, and its maximum corresponds to the *cis* conformer (Fig. S1 (Supporting Information)). For the *anti*-to-*cis* conformational interconversion, the positive signs for ΔE_{total}, ΔE_{Lewis} and ΔE_{deloc} indicate preference for the *anti* conformer. ΔE_{deloc} is 1/10 of ΔE_{Lewis}, showing that, in the absence of any steric effects, the electronic delocalization would favor the stabilization of both conformers. The delocalization effects are therefore less important for the rotation than the electrostatic and steric contributions included in the Lewis energy.

Table 2 shows the most important hyperconjugative interactions at the B3LYP/6-311++G(d,p) level resulting from the NBO analysis. It can be seen that the electronic charge transferred is greater in the *anti* conformer than in the *cis* conformer. This difference is due to the LP O(10) $\rightarrow \sigma^*$ C=O interaction, with a greater energy in the *anti* conformer (250.3 kJ mol^{-1}) than in the *cis* conformer (209.1 kJ mol^{-1}). The changes of bond lengths and bond angles going from the *anti* to the *cis* conformer have been calculated at the B3LYP/6-311++G(d,p) level. The calculated C(2)–O(10) bond length of $CF_3C(O)OCH_3$ increased from 1.327 pm in the *anti* conformer to 1.334 pm in the *cis* conformer, and the O=C–O bond angle decreased by 2.55°, due mainly to the lower LP O(10) $\rightarrow \sigma^*$ C=O interaction in the *cis* conformer than in the *anti* conformer.

Selected experimental geometrical parameters for $CF_3C(O)OCH_3$ are presented in Table S6 (Supporting Information) for comparison with those of the *anti, anti* conformer of $CF_3C(O)OCH_2CF_3$.[4] The shortening of the C(2)–O(10) bond by 0.8 pm and the C=O bond by 0.4 pm and the increase of the O=C–O bond angle by 4.4° in $CF_3C(O)OCH_3$ (*anti* conformer) relative to $CF_3C(O)OCH_2CF_3$ (*anti, anti* conformer) can be explained by the larger LP O(10) $\rightarrow \sigma^*$ C=O interaction in $CF_3C(O)OCH_3$ (250.3 kJ mol^{-1} compared with 232.8 kJ mol^{-1} in the heavier molecule).

Table 3. Refined (r_{h1}) and calculated[a] (r_e) geometric parameters for $CF_3CO_2CH_3$ from the GED study[b]

	Parameter	r_{h1}	r_e	Restraint
Independent				
p_1	*r*CF/CO/CC average	136.20(5)	136.13	–
p_2	*r*CF/CO/CC difference 1	21.2(2)	21.1	21.1(5)
p_3	*r*CF/CO/CC difference 2	13.5(3)	13.3	13.3(5)
p_4	*r*CF/CO/CC difference 3	5.3(4)	5.2	5.2(5)
p_5	*r*CF/CO/CC difference 4	6.0(4)	6.1	6.1(5)
p_6	*r*CF/CO/CC difference 5	12.0(4)	12.4	12.4(5)
p_7	*r*CH mean	108.9(4)	109.0	109.0(5)
p_8	∠OCH average	108.9(8)	107.5	107.5(10)
p_9	∠OCH difference	4.6(6)	4.8	4.8(6)
p_{10}	∠H(8)C(7)H(11)	111.2(9)	111.0	111.0(9)
p_{11}	∠C(2)O(10)C(7)	112.6(4)	114.2	–
p_{12}	∠O(10)C(2)C(1)	110.3(4)	109.1	–
p_{13}	∠CCF average	111.0(1)	110.6	–
p_{14}	∠CCF difference	0.0(4)	0.1	0.1(5)
p_{15}	∠F(3)C(1)F(4)	108.9(3)	108.5	108.5(6)
p_{16}	∠C(1)C(2)O(6)	122.1(4)	123.7	–
Dependent				
p_{17}	*r*C(2)=O(6)	120.8(2)	120.6	–
p_{18}	*r*C(2)–O(10)	132.8(3)	133.0	–
p_{19}	*r*C(7)–O(10)	144.4(3)	144.2	– –
p_{20}	*r*C(1)–C(2)	154.4(2)	154.2	–
p_{21}	*r*C(1)–F(3/5)	134.1(2)	134.0	–
p_{22}	*r*C(1)–F(4)	132.9(3)	132.9	–
p_{23}	∠O(10)C(7)H(8/9)	111.2(8)	109.9	–
p_{24}	∠O(10)C(7)H(11)	106.6(8)	105.1	–
p_{25}	∠C(2)C(1)F(3/5)	111.0(2)	110.5	–
p_{26}	∠C(2)C(1)F(4)	111.0(3)	110.6	–

[a] Refers to MP2/6-311++G(d,p) calculations.
[b] Distances (*r*) are in pm and angles (∠) are in degrees. See text for parameter definitions and Fig. 1 for atom numbering. The figures in parentheses are the estimated standard deviations of the last digits.

GED study

On the basis of the calculations described above [MP2/6-311++G(d,p)], a model with C_s symmetry was written describing the geometry of the most stable conformer in terms of 16 refinable parameters, comprising seven bond lengths and differences and nine angles and differences. The atom numbering used in the descriptions of the parameters is shown in Fig. 1 and the parameters are listed in Table 3.

The C–F, C–O, C=O and C–C distances were combined to give an overall average value and a series of differences (p_{1-6}). These

were defined as follows:

$$p_1 = \{[C(2)=O(6)] + [C(2)-O(10)] + [C(1)-F(4)] + 2 \times [C(1)-F(3)] + [C(7)-O(10)] + [C(1)-C(2)]\}/7$$

$$p_2 = [C(1)-C(2)] - \{[C(2)=O(6)] + [C(2)-O(10)] + [C(1)-F(4)] + 2 \times [C(1)-F(3)] + [C(7)-O(10)]\}/6$$

$$p_3 = [C(7)-O(10)] - \{[C(2)=O(6)] + [C(2)-O(10)] + [C(1)-F(4)] + 2 \times [C(1)-F(3)]\}/5$$

$$p_4 = [C(1)-F(3)] - \{[C(2)=O(6)] + [C(2)-O(10)] + [C(1)-F(4)]\}/3$$

$$p_5 = [C(1)-F(4)] - \{[C(2)=O(6)] + [C(2)-O(10)]\}/2$$

$$p_6 = [C(2)-O(10)] - [C(2)=O(6)]$$

A single mean C–H parameter (p_7) completed the set of distance parameters used in the model.

As the molecule has C_s symmetry, two different C–C–H angles must be defined and these were described as the average of the two and the corresponding difference (p_{8-9}). The H(8)C(7)H(11) angle was also defined (p_{10}). Other angles that were defined in the model included C(2)O(10)C(7) (p_{11}), O(10)C(2)C(1) (p_{12}) and C(1)C(2)O(6) (p_{16}). As with the methyl group, the C_s-symmetric CF_3 group was described using the average of two C–C–F angles, the difference between the two and the angle F(3)C(1)F(4) (p_{13-15}).

All 16 independent geometric parameters were refined by least squares. Restraints were applied, using the SARACEN method,[32] to parameters that could otherwise not be refined (Table 3). The restraints were based on values calculated at the MP2/6-311++G(d,p) level, and the uncertainties were derived from the changes in value of each parameter during the series of calculations that was performed. In addition, eight groups of amplitudes of vibration were refined. (See Table S7 in Supporting Information for a list of amplitudes of vibration and curvilinear distance corrections.)

The success of the refinement can be assessed numerically using the final R factor, which was $R_G = 0.039$ ($R_D = 0.018$), and visually using the goodness of fit of the radial distribution and difference curves, as seen in Fig. 5, and the molecular scattering intensity curves (Fig. S2, Supporting Information). The least-squares correlation matrix is given in Table S8 (Supporting Information), and coordinates for the final GED structures and for the calculated structures [MP2/6-311++G(d,p)] are given in Tables S9 and S10 (Supporting Information), respectively.

Vibrational study

Vibrational spectra of $CF_3C(O)OCH_3$ are shown in Fig. 6 (infrared spectra of the liquid and gas), Fig. 7 (polarized Raman spectrum of the liquid) and Fig. S3 (Supporting Information, far-infrared spectrum of the gas), while the wavenumbers corresponding to the observed spectral features are given in Table 4.

The wavenumbers of the 27 normal modes of vibration of $CF_3C(O)OCH_3$ (18 $A' + 9\ A''$) were calculated using the B3LYP functional, resulting the following root mean-square deviations (RMSD) from the experimental data for each basis set: 53.3 cm^{-1} for 6-31G(d); 42.9 cm^{-1} for 6-311G(d,p); 43.5 cm^{-1} for 6-311++G(d,p). The results obtained with the last mentioned basis set were used for the vibrational analysis, in order to facilitate the comparison of the results with those obtained previously for related molecules.[4]

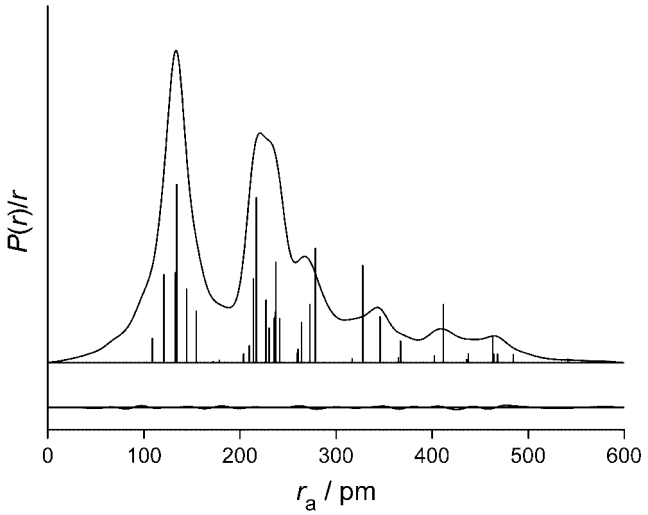

Figure 5. Experimental radial distribution curve and theoretical-minus-experimental difference curve for the refinement of $CF_3C(O)OCH_3$. Before Fourier inversion, the data were multiplied by $s \cdot \exp(-0.00002s^2)/(Z_O - f_O)(Z_F - f_F)$.

The gas band contours were helpful in confirming the assignment of bands to the different vibrational modes of the molecule. In fact, several bands show characteristic contours in the gas spectrum resulting from the unresolved rotational components.

Using the geometrical parameters given by the DFT calculation, the following values of the molecular main inertial moments were obtained: $I_A = 234.7$; $I_B = 557.9$; $I_C = 637.5 \times 10^{-40}$ g cm^2. The I_A inertial axis is almost parallel to the C–CF_3 bond, whereas the I_B axis is normal to I_A (in the symmetry plane) and the I_C axis is normal to that plane. Type-A bands resulting from vibrations leading to a variation of dipole moment (approximately) parallel to I_A will show a marked PQR structure, type-B bands will show a PQQR structure and type-C bands will show a prominent Q branch.[33] Type-A bands should show a PR separation of about 11.8 cm^{-1},[7] near to the mean value of 10.5 cm^{-1} measured in the gas spectrum of the studied substance. Vibrational modes of A' symmetry involving dipole changes in directions that are not approximately parallel to either the A or the B axis will have a hybrid AB structure.

The polarized Raman spectra at 0° and 90° with respect to the plane of polarization of the exciting light served also to confirm some assignments. The theoretical coefficients of depolarization are $0 \leq \rho_s < 3/4$ for the A' modes and $\rho_s = 3/4$ for the A'' modes. However, in this case this relation does not hold exactly and the observed values were $0 < \rho_s < 3/5$ for the A' modes and $\rho_s = 3/5$ for the A'' modes; hence, $\rho_{s\ antisim} > \rho_{s\ sim}$ which confirms the assignment carried out.

The assignment of the experimental bands to the normal modes of vibration of methyl trifluoroacetate was based mainly on comparison with data for related molecules and with the results of the quantum chemistry calculations. The following discussion refers mainly to the bands appearing in the gas-phase spectrum.

Assignment of bands

Methyl group modes

Three clearly defined bands appear in the IR and Raman spectra of the liquid substances in the range 3100–2950 cm^{-1} which are assigned to the expected CH_3 stretching modes. The weak bands

Journal of RAMAN SPECTROSCOPY

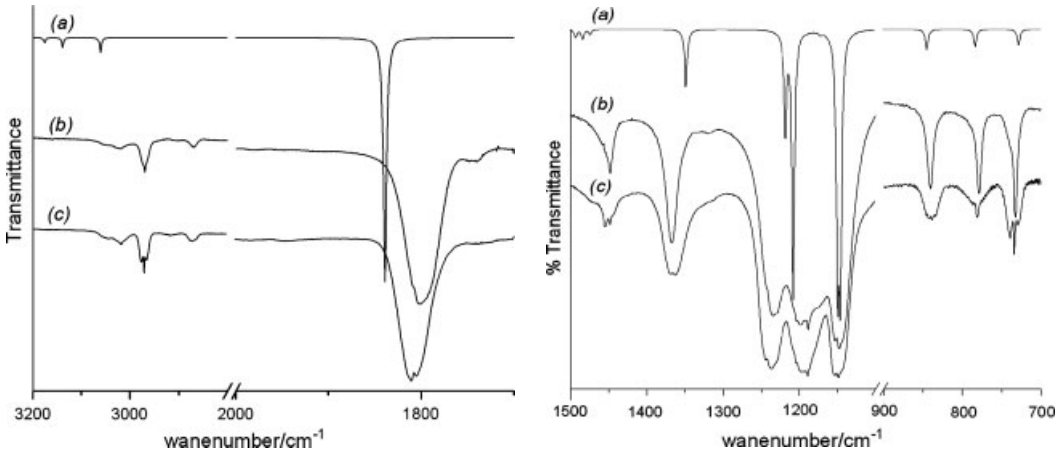

Figure 6. Infrared spectra of $CF_3C(O)OCH_3$. (a) The calculated spectrum; (b) The liquid phase; (c) The gas phase (path length: 10 cm, pressure: 5 Torr, resolution: 1 cm^{-1}).

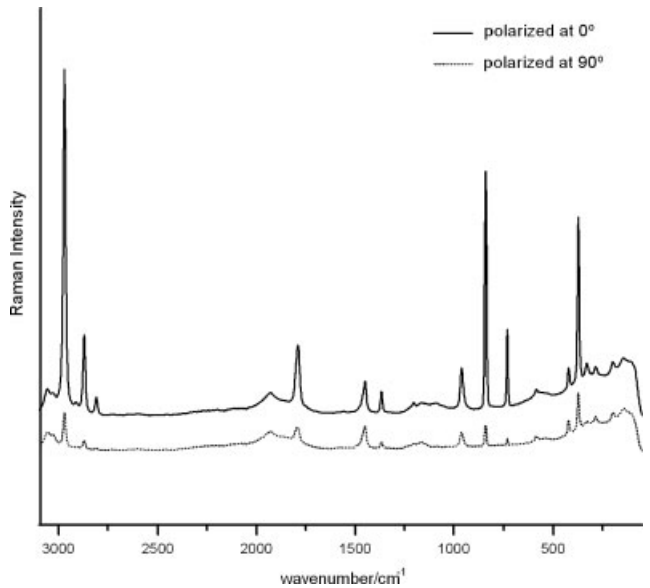

Figure 7. Polarized Raman spectra of liquid $CF_3C(O)OCH_3$ at room temperature (resolution: 4 cm^{-1}).

at 3044 and 3018 cm^{-1} are assigned to the CH_3 antisymmetric stretching modes of species A' and A'' respectively, because of their rotational envelopes (see band type in Table 5). The A-type band centred at 2970.1 cm^{-1} is assigned to the CH_3 symmetric stretching mode, being the Raman counterpart the most intense in the spectrum.

The bands centred at 1469 (shoulder), 1455 (C type) and 1448.6 cm^{-1} (AB type) should be assigned to the CH_3 bending modes. The last one, with a relatively intense counterpart in Raman, is assigned to the CH_3 symmetric bending mode. The 1455 cm^{-1} band is assigned to the antisymmetric deformation of A'' species because of its C-type contour, leaving the 1469 cm^{-1} shoulder to the similar mode of A' species. According to the calculations, the CH_3 rocking mode of species A' should give a relatively strong band in the infrared, which, however, should be severely overlapped by the stronger CF_3 stretching bands. A weak band located at 1203 cm^{-1} in the Raman spectrum, which probably correspond to the band observed at 1200 cm^{-1} by Jones *et al.*[5] in the infrared spectrum of the substance in CS_2 solution, is assigned to that mode. A weak and broad band centred at 1163 cm^{-1} in the Raman spectrum is assigned tentatively to the CH_3 rocking mode of species A'', which should be at lower frequencies (Table 5).

Carbonyl group modes

The strong band at 1806 cm^{-1} in the liquid infrared spectrum is immediately assigned to the C═O stretching mode. This band shows a type-B envelope, in agreement with a vibrational mode producing a dipole change quasi-parallel to the B inertial axis.

The band with a C-type contour located at 780.5 cm^{-1} is assigned to the out-of-plane rocking of the C═O group, in agreement also with the calculated value (Table 5). The in-plane rocking of the C═O group is associated with the A-type band centred at 420.6 cm^{-1}, also near the calculated value.

Trifluoromethyl group modes

The very strong infrared bands located between 1300 and 1100 cm^{-1} correspond to the three CF_3 stretching modes. The corresponding assignment was made mainly by comparison with $CF_3C(O)OH$[34] and with the calculations. On this basis, the very strong band centered at 1148.0 cm^{-1}, with a type-A contour, is assigned to the CF_3 symmetric stretch. In the same way, the bands located at 1237 and 1188.5 cm^{-1} are assigned to the CF_3 antisymmetric stretching modes of species A' and A'', respectively. The assignments of these bands by Jones *et al.*[5] are quite different.

The type-A band located at 733.5 cm^{-1} is assigned to the CF_3 symmetric deformation mode, which involves a dipole moment change parallel to the minor inertial axis. Besides, the Raman counterpart is clearly polarized. The bands at 585 cm^{-1} (B-type) and 524.6 cm^{-1} (C-type) are assigned to the CF_3 antisymmetric deformation modes of species A' and A'', respectively. Both the band contours and the calculated frequencies and relative intensities (Table 5) agree with that assignment.

The CF_3 rocking modes were assigned taking into account the theoretically predicted frequencies (Table 5). In that way, the bands located at 279.2 and 189 cm^{-1} are assigned to the CF_3 rocking modes of species A'' and A', respectively.

Table 4. Wavenumbers (in cm^{-1}) of the observed bands in the infrared and Raman spectra of $CF_3C(O)OCH_3$

Infrared[a]			Raman		
Gas	Band type	Liquid	Liquid[b]	Depolariz. coefficient[c]	Assignment
3044 br		3050 vw	3056 (11)	p 0.33	ν_1
3018 vw	C	3022 w	ca. 3026 (9)	dp 0.66	ν_{18}
2975.6 2970.1 w 2964.8	A	2970 w	2970 (100)	p 0.08	ν_2
1810.2 1804	B	1801 sh	1791 (23)	p 0.17	ν_3
1469 sh, br					ν_4
1455 w	C?	1455 w	–	p 0.33	ν_{19}
1448.3 w 1443 sh	AB	1448 w	1449 (16)	–	ν_5
1369 1363	B	1367 m	1367 (10)	p 0.17	ν_6
1237 vs		1234 vs	–	–	ν_7
Ca.1203 s		ca. 1201 s	1203	–	ν_8
1188.5 vs		1189 vs	1181	–	ν_{21}
–		ca.1174 sh	1163 (6) br	–	ν_{20}
1153.5 1148.0 1143 sh	A	1148 vs	–	–	ν_9
976 vw		961 vw	961 (18)	p 0.18	ν_{10}
838 w, br		841 w	841 (98)	p 0.07	ν_{11}
780.5 w	C	778 w	–	–	ν_{22}
738.7 733.5 m 728.8	A	732 m	732 (45)	p 0.08	ν_{12}
589 582	B	586 vw	586 (10)	–	ν_{13}
524.6 m	C	524 vw		–	ν_{23}
426.3 420.6 415.6	A	–	422 (21)	p 0.33	ν_{14}
375.4 370.0 364.5	A	–	372 (89)	p 0.16	ν_{15}
329 m		–	328 (19)	p 0.33	ν_{16}
279.2 m	C?	–	285 (19)	dp 0.40	ν_{24}
Ca. 189 w, br		–	197 (21)p	p 0.29	ν_{17}
Ca. 133 w, br		–	143 (22)	dp 0.50	ν_{25}

[a] sh, shoulder; s, strong; w, weak; m, medium; v, very.
[b] Relative band heights in parentheses.
[c] p, polarized; dp, depolarized.

Skeletal modes

The C–C–O–C skeletal bonds generate stretching modes in which the three bonds are strongly coupled. According to the calculated displacement vectors, the 1366 cm^{-1} band is assigned to the out-of-phase C–C–O stretching (calculated: 1349 cm^{-1}) and the 838 cm^{-1} band is associated with the corresponding in-phase stretching (calculated: 844 cm^{-1}); the many components in the potential energy distribution for these vibrational modes point to the complexity of such movements. Finally, the weak 976 cm^{-1} band should be assigned to the O–CH_3 stretching movement (calculated: 974 cm^{-1}). It should be remarked that the assignment of the 1366 cm^{-1} band does not agree with previous proposals.[6,7]

The calculations indicate that the A-type band located at 370 cm^{-1} should be assigned to a mode in which there is a minor contribution of the CCO and COC angles, whereas the more intense 329 cm^{-1} band should be assigned to the COC deformation mode. The calculated frequencies and intensities agree with the observed bands (Table 5).

Torsional modes

The molecule has three low-frequency torsional modes. However, only one weak and broad band located at 133 cm^{-1} in the FIR spectrum could be assigned to the O–C(O) torsional mode.

Calculation of force constants

The Cartesian force field for $CF_3C(O)OCH_3$ resulting from the B3LYP/6-311++G(d,p) calculations were transformed to the set of non-redundant natural coordinates defined in Table S11 (Supporting Information). Such coordinates take into account the local symmetry around the C atoms and follow the proposals of Fogarasi *et al.*[23] The resulting force field was subsequently scaled using the scheme proposed by Pulay *et al.*[8] (see Computational

Table 5. Observed and calculated wavenumbers, infrared and Raman intensities and potential energy distribution for the *anti* conformer of $CF_3C(O)OCH_3$

Mode	Observed	Calculated[a]	Calculated SQM[b]	IR intensity[c]	Raman activity[d]	PED (contributions ≥10%)[e]	Approximate description
A′							
ν_1	3044	3176	3049	6.82	59.18	$93S_1$	ν CH_3 antis.
ν_2	2970	3060	2972	18.37	135.72	$94S_2$	ν CH_3 sim.
ν_3	1807	1839	1809	285.73	9.19	$97S_3$	ν C=O
ν_4	1469	1493	1469	10.55	5.25	$84S_4 + 16S_7$	δ CH_3 antis.
ν_5	1448	1474	1448	6.13	2.19	$84S_5$	δ CH_3 sim.
ν_6	1366	1349	1350	75.87	2.05	$17S_5 + 32S_6 + 14S_9 + 33S_{11} + 14S_{12} + 16S_{14}$	ν (O)C–O
ν_7	1237	1217	1227	140.52	2.24	$12S_4 + 65S_7$	ρ CH_3
ν_8	1203	1207	1225	388.84	0.64	$88S_8 + 16S_{13}$	ν CF_3 antis.
ν_9	1148	1148	1154	305.02	1.12	$23S_6 + 32S_9 + 11S_{10} + 25S_{12} + 10S_{14}$	ν CF_3 sim.
ν_{10}	976	974	977	7.77	5.32	$89S_{10}$	ν O–CH_3
ν_{11}	838	844	850	25.78	6.93	$19S_6 + 15S_9 + 17S_{14} + 16S_{16}$	ν C–C
ν_{12}	734	728	733	20.25	2.70	$33S_9 + 37S_{12}$	δ CF_3 sim.
ν_{13}	585	574	583	0.79	1.60	$13S_8 + 36S_{13}$	δ CF_3 antis.
ν_{14}	421	415	423	1.91	1.30	$45S_{13} + 18S_{14} + 13S_{15} + 18S_{17}$	wag. C=O in-pl.
ν_{15}	370	367	369	3.56	3.71	$36S_{11} + 20S_{12}$	δ CCO
ν_{16}	329	315	325	15.84	0.72	$21S_{14} + 51S_{16} + 30S_{17}$	δ COC
ν_{17}	189	182	186	0.94	0.28	$58S_{15} + 21S_{16} + 30S_{17}$	ρ CF_3
A″							
ν_{18}	3018	3139	3010	11.88	40.14	$100S_{18}$	ν CH_3 antis.
ν_{19}	1455	1484	1456	12.63	9.40	$93S_{19}$	δ CH_3 antis.
ν_{20}	1163	1171	1163	3.74	2.64	$56S_{20} + 38S_{21}$	ρ CH_3
ν_{21}	1189	1145	1159	303.69	1.62	$38S_{20} + 63S_{21} + 12S_{24}$	ν CF_3 antis.
ν_{22}	781	783	779	21.97	0.05	$61S_{22} + 13S_{24}$	wag. C=O out-pl.
ν_{23}	525	519	525	5.82	0.79	$78S_{23}$	δ CF_3 antis.
ν_{24}	279	283	285	5.97	0.61	$12S_{22} + 64S_{24} + 20S_{25}$	ρ CF_3
ν_{25}	133	131	131	0.69	0.12	$22S_{22} + 21S_{24} + 66S_{25}$	τ C–O
ν_{26}	–	103	105	0.47	0.44	$15S_{25} + 85S_{26}$	τ CH_3
ν_{27}	25[f]	25	25	1.48	0.64	$100S_{27}$	τ CF_3
RMSD/cm^{-1}		42	9				

[a] B3LYP/6-311++G(d,p) calculation.
[b] From Scaled Quantum Mechanics force field.
[c] Infrared intensities in km mol^{-1}.
[d] Raman activities in $Å^4$ amu^{-1}.
[e] Coordinate numbers correspond to Table S11 (Supporting Information).
[f] From Ref. [5]

details). All of the initial scale factors were taken as unity for all modes and were subsequently modified by a least-squares procedure to obtain the best fit to the experimental frequencies, as shown in Table S12 (Supporting Information). All vibrational wavenumbers were assigned the same weight in the adjustment, and no empirical correction of the theoretical geometry was used. The resulting SQM force field (Table S13 (Supporting Information)) served to calculate the potential energy distribution for the molecule. The final RMSD and potential energy distribution are presented in Table 5. It can be seen that only about one-half of the modes have a participation of 50% or more of one defined coordinate, whereas other modes represent complex vibrations in which several coordinates are involved.

The SQM force field was used to calculate the internal force constants shown in Table S14 (Supporting Information), where they are compared with the equivalent values for the previously studied trifluoroethyl trifluoroacetate.[4] There is an increase in the stretching force constants on moving from $CF_3C(O)OCH_3$ to $CF_3C(O)OCH_2CF_3$, with the exception of the decreasing *f*[C(2)–O(10)]. These differences are in accordance with the corresponding differences in the bond lengths (Table 3), although the C=O bond shows an anomalous behaviour.

Conclusions

A complete investigation of the molecular structure of $CF_3C(O)OCH_3$ in the gas phase has been carried out by electron diffraction, complemented by theoretical methods. The GED experimental data shows that this molecule exists at room temperature as a single *anti* conformer having a CCOC dihedral angle of 180°. The theoretical methods indicate two possible conform-

ers, *anti* and *cis*, with CCOC dihedral angles of 180° and 0.5° respectively, the first one being the most stable.

The decomposition of the potential energy function as a Fourier expansion and the analysis of different terms (V_i) has been shown to be useful in analysing the relative stabilities of different conformations of molecular systems. V_1 and V_2 are the main terms of the Fourier expansion. It is concluded that the steric effects show a preference for the *anti* conformer, while the hyperconjugative effects stabilize both conformers. The greater stability of the *anti* conformer with respect to the *cis* conformer shows that the delocalization contributions are less important than the electronic and steric effects.

Infrared and Raman spectra for $CF_3C(O)OCH_3$ show bands assignable to 25 out of the expected 27 normal modes of vibration. Using the observed frequencies, it was possible to scale the theoretical force field; the resulting SQM force field served to calculate the potential energy distribution, which revealed the physical nature of the molecular vibrations and the force constants in internal coordinates.

Acknowledgements

We acknowledge research grants from CIUNT (Consejo de Investigaciones de la Universidad Nacional de Tucumán), CONICET (Consejo Nacional de Investigaciones Científicas y Técnicas, PIP 6457 and 5633), ANPCYT (Agencia Nacional de Promoción Científica y Tecnológica, BID 1728/OC-AR, PICT 11127) and UNLP (Universidad Nacional de La Plata). We also thank the EPSRC for funding the programme of electron-diffraction research (Grant No: EP/C513649) and the NSCCS for computational resources. We are grateful to Dr. A. Navarro (Universidad de Jaen, Spain) for running the Raman spectrum and Dr. R. Romano (Universidad de La Plata, R. Argentina) for obtaining the far infrared spectrum.

Supporting information

Supporting information may be found in the online version of this article.

References

[1] D. W. Nelson, J. Owens, D. Hiraldo, *J. Org. Chem.* **2001**, *66*, 2572.
[2] J. J. Yang, R. L. Kirchmeier, J. M. Shreeve, *J. Org. Chem.* **1998**, *63*, 2656.
[3] V. Y. Sosnovskikh, B. I. Usachev, D. V. Sevenard, G. V. Röschenthaler, *J. Org. Chem.* **2003**, *68*, 7747.
[4] M. E. Defonsi Lestard, M. E. Tuttolomondo, E. L. Varetti, D. A. Wann, H. E. Robertson, D. W. H. Rankin, A. Ben Altabef, *J. Mol. Struct.* **2009**, *917*, 183.
[5] G. I. L. Jones, T. D. Summers, N. L. Owen, *J. Chem. Soc., Faraday Trans. 2* **1974**, *70*, 100.
[6] A. G. Robiette, J. C. Thompson, *Spectrochim. Acta Part A* **1965**, *21*, 2023.
[7] G. A. Crowder, D. Jackson, *Spectrochim. Acta Part A* **1971**, *27*, 1873.
[8] P. Pulay, G. Fogarasi, G. Pongor, J. E. Boggs, A. Braga, *J. Am. Chem. Soc.* **1983**, *105*, 7037.
[9] C. M. Huntley, G. S. Laurenson, D. W. H. Rankin, *J. Chem. Soc., Dalton Trans.* **1980**, *9*, 954.
[10] H. Fleischer, D. A. Wann, S. L. Hinchley, K. B. Borisenko, J. R. Lewis, R. J. Mawhorter, H. E. Robertson, D. W. H. Rankin, *Dalton Trans.* **2005**, *19*, 3221.
[11] S. L. Hinchley, H. E. Robertson, K. B. Borisenko, A. R. Turner, B. F. Johnston, D. W. H. Rankin, M. Ahmadian, J. N. Jones, A. H. Cowley, *Dalton Trans.* **2004**, *16*, 2469.
[12] W. Ross, M. Fink, R. Hilderbrandt, *International Tables for Crystallography*, vol. C (Ed.: A. J. C. Wilson), Kluwer Academic Publishers: Dordrecht, Netherlands, **1992**, p 245.
[13] National Service for Computational Chemistry Software (NSCCS), **2001**, http://www.nsccs.ac.uk.
[14] M. J. Frisch, G. W. Trucks, H. B. Schlegel, G. E. Scuseria, M. A. Robb, J. R. Cheeseman, J. A. Montgomery Jr., T. Vreven, K. N. Kudin, J. C. Burant, J. M. Millam, S. S. Iyengar, J. Tomasi, V. Barone, B. Mennucci, M. Cossi, G. Scalmani, N. Rega, G. A. Petersson, H. Nakatsuji, M. Hada, M. Ehara, K. Toyota, R. Fukuda, J. Hasegawa, M. Ishida, T. Nakajima, Y. Honda, O. Kitao, H. Nakai, M. Klene, X. Li, J. E. Knox, H. P. Hratchian, J. B. Cross, C. Adamo, J. Jaramillo, R. Gomperts, R. E. Stratmann, O. Yazyev, A. J. Austin, R. Cammi, C. Pomelli, J. W. Ochterski, P. Y. Ayala, K. Morokuma, G. A. Voth, P. Salvador, J. J. Dannenberg, V. G. Zakrzewski, S. Dapprich, A. D. Daniels, M. C. Strain, O. Farkas, D. K. Malick, A. D. Rabuck, K. Raghavachari, J. B. Foresman, J. V. Ortiz, Q. Cui, A. G. Baboul, S. Clifford, J. Cioslowski, B. B. Stefanov, G. Liu, A. Liashenko, P. Piskorz, I. Komaromi, R. L. Martin, D. J. Fox, T. Keith, M. A. Al-Laham, C. Y. Peng, A. Nanayakkara, M. Challacombe, P. M. W. Gill, B. Johnson, W. Chen, M. W. Wong, C. González, J. A. Pople, *Gaussian 03, revision C.02*, Gaussian, Inc., Wallingford, **2004**.
[15] C. Møller, M. S. Plesset, *Phys. Rev.* **1934**, *46*, 618.
[16] (a) R. Krishnan, J. S. Binkley, R. Seeger, J. A. Pople, *J. Chem. Phys.* **1980**, *72*, 650; (b) A. D. McLean, G. S. Chandler, *J. Chem. Phys.* **1980**, *72*, 5639.
[17] W. J. Hehre, Pv. R. Schleyer, J. A. Pople, *Ab Initio Molecular Orbital Theory*, Wiley: New York, **1986**.
[18] D. Becke, *J. Chem. Phys.* **1993**, *98*, 5648.
[19] C. Lee, W. Yang, R. G. Parr, *Phys. Rev. B* **1988**, *37*, 785.
[20] C. Alamo, V. Barone, *J. Chem. Phys.* **1998**, *108*, 664.
[21] (a) V. A. Sipachev, *J. Mol. Struct. (THEOCHEM)* **1985**, *121*, 143; (b) V. A. Sipachev, *J. Mol. Struct.* **2001**, *567*, 67.
[22] E. D. Glendening, J. K. Badenhoop, A. D. Reed, J. E. Carpenter, F. F. Weinhold, *Theoretical Chemistry Institute*, University of Wisconsin: Madison, **1996**.
[23] G. Fogarasi, X. Zhou, P. W. Taylor, P. Pulay, *J. Am. Chem. Soc.* **1992**, *114*, 8191.
[24] E. B. Wilson, J. C. Decius, P. C. Cross, *Molecular Vibrations*, McGraw-Hill: New York, **1955**.
[25] W. B. Collier *Program FCARTP (QCPE #631)*, Department of Chemistry, Oral Roberts University: Tulsa, **1992**.
[26] B. Nielsen, A. J. Holder, *GaussView, User's Reference*, GAUSSIAN Inc.: Pittsburgh, **1997–1998**.
[27] J. L. Duncan, *Mol. Phys.* **1974**, *28*, 1177.
[28] S. Millefiori, A. Alparone, *J. Chem. Soc., Faraday Trans.* **1998**, *94*, 25.
[29] L. Radom, W. J. Hehre, J. A. Pople, *J. Am. Chem. Soc.* **1972**, *94*, 2371.
[30] L. Radom, J. A. Pople, *J. Am. Chem. Soc.* **1970**, *92*, 4786.
[31] D. Bond, Pv. R. Schleyer, *J. Org. Chem.* **1990**, *55*, 1003.
[32] N. W. Mitzel, D. W. H. Rankin, *Dalton Trans.* **2003**, *19*, 3650.
[33] T. Ueda, T. Shimanouchi, *J. Mol. Spectrosc.* **1968**, *28*, 350.
[34] R. L. Redington, K. C. Lin, *Spectrochim. Acta Part A* **1971**, *27A*, 2445.